Pressure Measurements for Monitoring CO$_2$ Foam Pilots

Metin Karakas [1,*], Zachary Paul Alcorn [1], Fred Aminzadeh [2] and Arne Graue [1]

[1] Department of Physics and Technology, University of Bergen, P.O. Box 7803, 5007 Bergen, Norway; zachary.alcorn@uib.no (Z.P.A.); arne.graue@uib.no (A.G.)

[2] FACT Inc., 3345 State St., Suite 3282, Santa Barbara, CA 93130-7001, USA; fred.aminzadeh@fact-corp.com

[*] Correspondence: metin.karakas@uib.no; Tel.: +1-310-795-5980

Abstract: This study focuses on the use of pressure measurements to monitor the effectiveness of foam as a CO$_2$ mobility control agent in oil-producing reservoirs. When it is applied optimally, foam has excellent potential to improve reservoir sweep efficiency, as well as CO$_2$ utilization and storage, during CO$_2$ Enhanced Oil Recovery (EOR) processes. In this study, we present part of an integrated and novel workflow involving laboratory measurements, reservoir modeling and monitoring. Using the recorded bottom-hole pressure data from a CO$_2$ foam pilot study, we demonstrate how transient pressures could be used to monitor CO$_2$ foam development inside the reservoir. Results from a recent CO$_2$ foam pilot study in a heterogeneous carbonate field in Permian Basin, USA, are presented. The injection pressure was used to evaluate the development of foam during various foam injection cycles. A high-resolution radial simulator was utilized to study the effect of foam on well injectivity, as well as on CO$_2$ mobility in the reservoir during the surfactant-alternating gas (SAG) process. Transient analysis indicated constant temperature behavior during all SAG cycles. On the other hand, differential pressures consistently increased during the surfactant injection and decreased during the subsequent CO$_2$ injection periods. Pressure buildup during the periods of surfactant injection indicated the development of a reduced mobility zone in the reservoir. The radial model proved to be useful to assess the reservoir foam strength during this pilot study. Transient analysis revealed that the differential pressures during the SAG cycles were higher than the pressures observed during the water-alternating gas (WAG) cycle which, in turn, showed foam generation and reduced CO$_2$ mobility in the reservoir. Although pressure data are a powerful indicator of foam strength, additional measurements may be required to describe the complex physics of in situ foam generation. In this pilot study, it appeared that the reservoir foam strength was weaker than that expected in the laboratory.

Keywords: CO$_2$ foam; pilot monitoring; pressure measurements; transient analysis; CO$_2$ EOR; CO$_2$ storage

1. Introduction

CO$_2$ foam injection is an effective method for controlling CO$_2$ mobility during enhanced oil recovery (EOR) processes in petroleum reservoirs [1]. When it is performed optimally, CO$_2$ foam has excellent potential to improve sweep efficiency [2–8] and CO$_2$ storage potential. Foam is a mixture consisting of a continuous liquid phase (surfactant solution) and a gas phase (CO$_2$). This mixture becomes discontinuous due to the generation of thin liquid films called lamellae [9]. The mobility of foam depends on its texture: the finer the foam's texture, the lower the CO$_2$ mobility. It has been shown that foam density is a direct function of the density of the lamellae [10]. Laboratory studies clearly show that foam strength is very important in achieving the desired reservoir displacement efficiency. Additionally, the solubility of the surfactant in CO$_2$ and water phases, as well as the adsorption of CO$_2$ on rocks, play a crucial role during foam displacement [11].

Surfactants are commonly used to generate and stabilize foams in porous media. They are screened to ensure the success of a CO$_2$ foam. Recent research has suggested various

surfactants (cationic, nonionic, and zwitterionic) as the main candidates for CO_2 foams in EOR [12]. Several studies have been conducted to examine the texture and stability of CO_2 foams as a function of the surfactant structure and formulation. These variables include the water/CO_2 ratio, surfactant concentration, water salinity, etc. Previous research shows that surfactant characteristics, along with foam strength, can be adjusted to ensure optimum foam displacement during CO_2 EOR processes. However, surfactant-based foams break down in the formation due to the presence of oil and the adsorption of the surfactant to rock, and at high temperatures and salinities. Therefore, it is also important to maintain foam strength (or stability) during the entire injection period in field applications. Recent work suggests that the addition of silica nanoparticles to surfactant-stabilized CO_2 foams may increase the strength and stability of foam systems [13].

There are several strategies to generate foam in porous media. These include the co-injection of gas (CO_2)/surfactant or surfactant-alternating gas (CO_2) injection (the SAG method). In the co-injection process, the gas (CO_2) and the surfactant solution are simultaneously injected, and foam is formed in situ. In the SAG method, the surfactant and CO_2 are injected in alternating slugs. In low-permeability reservoirs, SAG injection may be preferred due to increased gas injectivity. Additionally, with the use of the SAG method, the contact between CO_2 and water is minimized, which may reduce corrosion in surface facilities and piping [14].

Laboratory studies using reservoir cores are used to define the optimum recipe at a given reservoir pressure, temperature, and water salinity. For the application of foam in reservoirs where heterogeneity is involved, reservoir monitoring is carried out to assess foam development under reservoir conditions. While seismic, resistivity, electromagnetic and pressure measurements have been suggested in the oil industry, foam monitoring is typically carried out through flow and bottom hole pressure measurements, injection logging and the use of fluid tracers. These measurements are, in turn, used to assess the effectiveness of foam as a mobility control method and, hence, provide a way in which to remedy any underperforming CO_2 floods. In this way, the design of the foam can be adjusted to improve oil recovery, CO_2 utilization and storage.

In this study, we present the pressure monitoring part of an integrated and novel workflow involving laboratory measurements, reservoir modeling and monitoring. The laboratory studies were conducted on reservoir core samples to determine the optimal foam formulation. Reservoir modeling was carried out to decide on optimum injection strategy, and extensive reservoir monitoring was conducted to assess the effectiveness of the designed foam under reservoir conditions. The results of this integrated research work provide important knowledge for future CO_2 EOR field applications.

2. Pressure Testing for Foam Monitoring

In the petroleum industry, transient pressure testing is typically used to investigate reservoir characteristics such as permeability, reservoir boundaries, etc., as well as the well performance such as productivity or injectivity, skin effects, etc. Fall-off testing is an effective method for monitoring water or foam injection. Typically, fall-off tests are conducted by ceasing the injection and analyzing the transient pressure to assess any mobility changes near the injector [15]. In such tests, bottom-hole pressures are recorded at the injection well, and the data are used to examine the reservoir mobility changes caused by the injection. Foam injection affects the mobility distribution in the reservoir; therefore, the location of the foam front can be monitored, in principle, by fall-off tests. These tests rely on single-point pressure measurements and may lack the resolution required in layered formations.

Based on previous comparable studies with CO_2 injections [16], it has been suggested that crosswell pressure testing, in addition to seismic and electromagnetic data, could be deployed for CO_2 foam monitoring. In crosswell pressure testing, a series of pressure pulses is induced by shutting down the injector, and the pressure measurements are taken at the observation well. These measurements could be used to examine the inter-well

reservoir connectivity. The main advantage of these tests is the larger investigation volume away from the injector.

3. Field Pilot Description

A surfactant-stabilized foam was chosen to reduce the CO_2 mobility in this field. The surfactant system was selected based on laboratory measurements of surfactant adsorption. The foam stability was also verified during these laboratory studies. A surfactant-alternating gas (SAG) injection strategy was adapted, with 10 days of surfactant solution injection followed by 20 days of CO_2 injection. The pilot injection began in May 2019. Monitoring surveys during this pilot study included CO_2 injection profiles, CO_2 tracer tests, the collection of bottom-hole injection pressure/temperature and three-phase flow rates.

The pilot study was performed in the East Seminole Field, Permian Basin, West Texas, and the study area was an inverted 40 acre 5-spot pattern which included a central injection well and four surrounding producers (Figure 1). The oil was produced from the San Andres formation, which is classified as a heterogeneous cyclical carbonate. The reservoir interval had an average permeability of 13 mD, pay thickness of 110 ft, and consisted of six flow zones separated by impermeable flow barriers. The pilot area was selected based on rapid CO_2 breakthrough, high GORs in the producers as well as relatively short well distances [17,18]. Two production wells, P1 and P4, were the focus of the baseline data collection and pilot monitoring because they exhibited the most rapid CO_2 breakthrough time from tertiary CO_2 injection. Composite logs from the pilot injection well indicated a 10 ft thick high permeability streak of 200 mD. Historical injection profiles showed that this zone has been taking most of the injected CO_2. Therefore, this high permeability zone was targeted because foam can form in high permeability streaks and diverting flow to unswept regions of the reservoir with lower permeabilities. The reservoir and fluid properties are shown in Table 1.
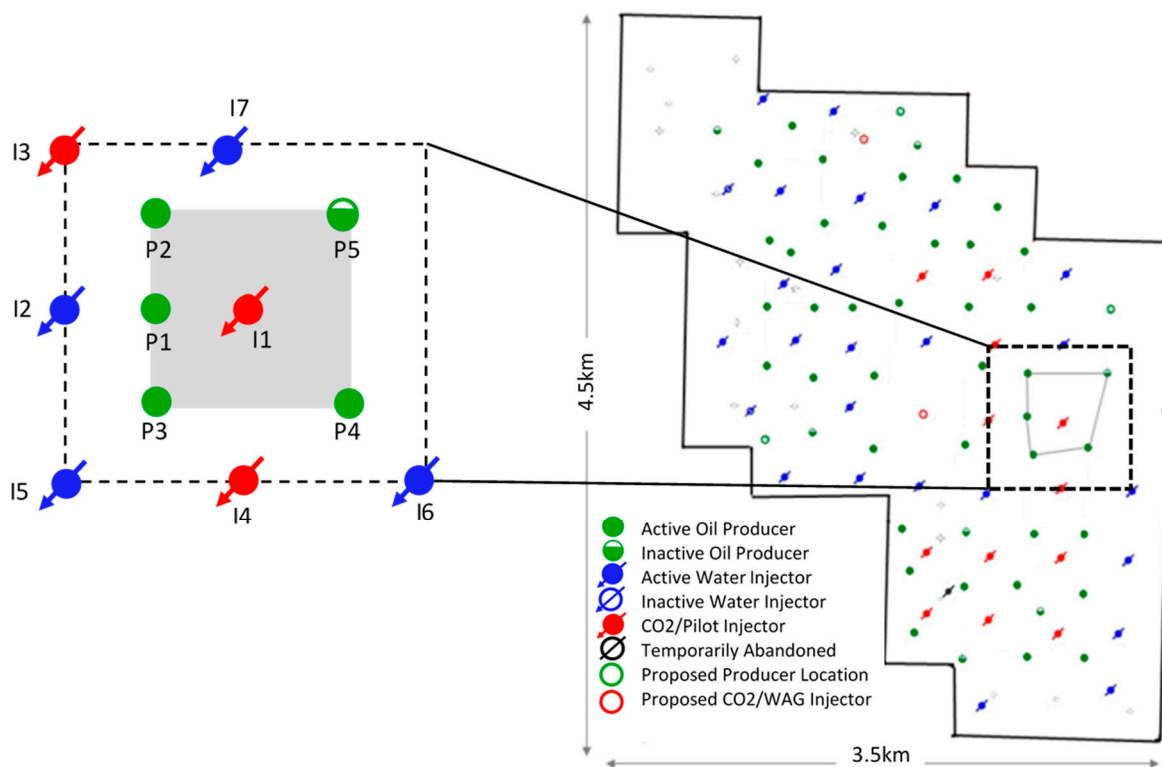

Figure 1. Pilot pattern (shaded area) and surrounding wells in East Seminole Field. The pilot injection well was I1, and the monitored producers were P1 through P4.

Table 1. Reservoir and fluid properties of the San Andres unit in the East Seminole Field.

Reservoir Characteristic	Value
Depth	5200 ft
Permeability	1 to 300 md (average: 13 md)
Porosity	3 to 28% (average: 12%)
Pay thickness	110 ft
Reservoir pressure (initial)	2500 psig
Reservoir pressure (current)	3400 psig
Fracture pressure	3900 psig
Reservoir temperature	104^0F
Oil gravity	31 °API
Formation brine salinity	70,000 ppm

4. Foam Formulation Design

The laboratory program aimed to determine the optimal foam formulation for the field test. This included surfactant-screening studies, evaluations of the optimal foam quality (gas fraction) and surfactant concentration and quantification of CO_2 EOR and CO_2 storage potential. Individual components of the laboratory program have been detailed elsewhere [12,13,17,18] and are briefly reviewed here.

Surfactant screening studies identified the nonionic water-soluble Huntsman L24-22, a linear ethoxylated alcohol (C12-14 EO22), for the field pilot study based upon minimal loss to the formation due to adsorption, adequate foam strength, and chemical stability [12]. Once the reservoir-specific surfactant was selected, the foam formulation was evaluated by determining the impact of surfactant concentration, gas fraction (foam quality) and flow velocity on foam strength at reservoir conditions [18]. The foam strength was quantitatively evaluated by the apparent foam viscosity, which was calculated from the steady-state pressure gradient at each gas fraction during foam quality scans and at each injection rate during foam rate scans [19]. As described in Section 6, foam model parameters for numeral modeling were derived from the foam quality and foam rate scans by curve-fitting regression [20–22].

5. Radial Model Set-Up and Initialization

In this pilot study, injection well pressures and temperatures were recorded using a down-hole memory pressure gauge during various surfactant, CO_2 and water injection periods. The transient analysis was conducted by examining the differential pressure (dP) and differential temperature (dT) over time for nine SAG cycles and one WAG cycle. A high-resolution two-dimensional radial foam simulator was used to history-match the measured transient pressure data. The simulation model included the porosity and permeability distribution from a validated sector-scale model of the pilot pattern and surrounding producers [21]. The simulation foam model was used to examine the impact of foam and/or relative permeability on injectivity and mobility reduction when switching between surfactant solution and CO_2 in an SAG process.

The objectives of this study were as follows:

- Evaluate whether foam has been generated based upon comparisons with measured BHP and injection rates;
- Tune foam model to observed pressures during pilot if foam has formed;
- Determine the foam propagation distance/rate if foam has formed.

The radial model used in this study was based upon a validated sector-level model of the pilot pattern and surrounding producers. The base sector model was calibrated to 40 years of waterflood and over 4 years of CO_2 injection data, before the pilot study. A workflow was developed to history-match the cumulative oil production and water-cut in the sector model [22].

The radial model included one injector (I1) which simulated the nine-cycle SAG pilot period. The grid contained 28 layers, which were refined from the validated sector model of

the pilot pattern and surrounding wells. The radial grid extended to 700 ft from the injector and the grid sizes increased logarithmically from the injector. Layers and perforations were from the history-matched (HM) sector model (reference to Mohan's PhD/papers with HM models). The model included historical water and CO_2 injections before the pilot study. The simulations during the pilot study were controlled by the actual injection rates, and the simulated rates were compared with historical rates to ensure that the model could adhere to these controls.

Figure 2 shows the permeability distribution in the radial model. Radial simulation model parameters are provided in Table 2.
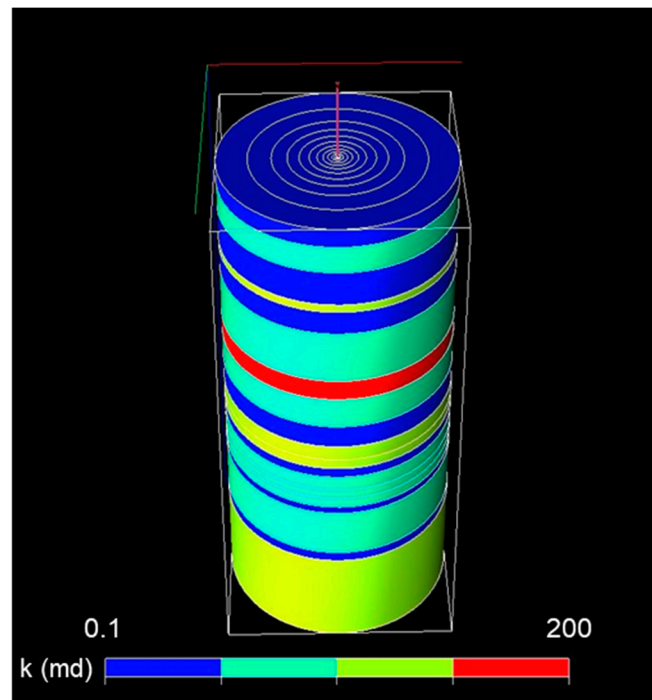

Figure 2. Permeability distribution in the radial model. The number of radial and vertical grid blocks are 20 and 28, respectively.

Table 2. Radial simulation model parameters.

Simulation Model Parameter	
Number of grid blocks	$20 \times 1 \times 28$ (r, theta, z)
Outer radius	700 ft
Total thickness	145 ft
Initial water saturation (Sw)	0.50
Starting reservoir pressure	3118 psia
Fracture pressure	3900 psig
Reservoir temperature	104^0F
Oil gravity	31 °API
Formation brine salinity	70,000 ppm
Permeability and porosity from the HM sector model	
Average permeability	13.5 md
Average porosity	0.08
Initial conditions on 1 April 2019.	

Base values for foam model parameters were obtained by performing regression analysis on the quality scan data to fit the empirical foam model [21,23]. Figure 3 shows the foam characteristics obtained based on the regression analysis.
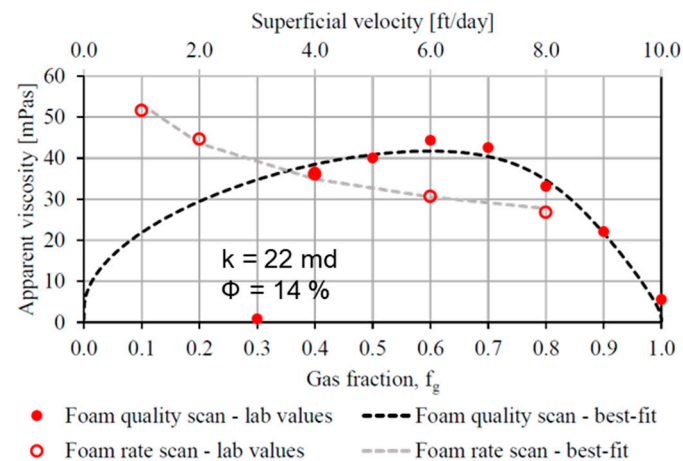
Figure 3. Laboratory foam quality (red filled circles) and rate (red open circles) scans used to derive foam model parameters for the local equilibrium foam model. The dashed lines show the model fit.

The simulation model was run using daily pilot study injection rates using the rate control option of the simulator.

6. Foam Modeling

There are two approaches to modeling foam transport in porous media: an explicit texture population balance model [10,24].and an implicit texture local equilibrium model [25,26]. Population balance models explicitly represent the dynamics of lamella creation and destruction along with the effect of the resulting foam on gas mobility. Gas mobility is reduced according to bubble size (determined by the rates of creation and destruction of lamellae). Local equilibrium models implicitly represent the effect of bubble size by introducing factors for reducing gas mobility by foam as a function of water saturation, oil saturation, surfactant concentration, and shear thinning due to the flow rate. Local equilibrium models assume that foam is present anywhere gas and water are present, along with an adequate surfactant concentration. The effect of foam was modeled in this study using the local equilibrium approach.

The decrease in gas mobility during foam floods is accounted for in local equilibrium models by scaling the gas relative permeability for no foam floods ($k_{rg}{}^{nf}$) by a mobility reduction factor (*FM*), whereas the water relative permeabilities remain unchanged.

$$k_{rg}^{f} = k_{rg}^{nf} \times FM \tag{1}$$

The effect of water saturation, shear rate, surfactant concentration and oil saturation [26] on the mobility reduction factor was studied, given by the expression:

$$FM = \frac{1}{1 + fmmmob \times F_{water} \times F_{shear} \times F_{oil} \times F_{surf}} \tag{2}$$

fmmmob refers to the maximum gas mobility reduction that can be achieved. F_{water}, F_{shear}, F_{oil} and F_{surf} capture the water saturation, shear rate, oil saturation and surfactant concentration dependence, respectively, all lying in the range of 0 to 1 (Equations (3) through (6)). The capillary number, N_{ca}, represents the relative effect of viscous and capillary forces.

$$F_{water} = 0.5 + \frac{arctan[epdry(S_w - fmdry)]}{\pi} \tag{3}$$

$$F_{shear} = \begin{cases} \left(\frac{fmcap}{Nca}\right)^{epcap} & if\ N_{ca} > fmcap \\ 1\ otherwise \end{cases} \tag{4}$$

$$F_{surf} = \left(\frac{Surfactant\ concentration}{fmsurf} \right)^{epsurf} \tag{5}$$

$$F_{oil} = \left(\frac{fmoil - So}{fmoil} \right)^{epoil} \tag{6}$$

Two water components were used to model foam behavior: one for surfactant solution and one for water. The base case foam parameters were derived from laboratory foam quality and rate scans and fitted to the empirical local equilibrium foam model by curve-fitting regression [19–21,25–27].

The surfactant selected for the pilot was found to have very low adsorption reservoir rock in the laboratory; thus, adsorption was excluded from the simulation study. Figure 3 shows the foam quality and rate scan used to derive the model parameters, and Table 3 shows the base case foam model parameters.

Table 3. Base case foam parameters.

Foam Parameter	Value
fmmob	192
fmdry	0.40
epdry	84
fmcap	9.0×10^{-7}
epcap	0.59

7. Measured Injection Rates and Pressures

The reservoir response to foam was evaluated by analyzing the bottom-hole pressure (BHP) response during surfactant and CO_2 injection. Figure 4 shows the injection rates of the CO_2 (red curve) and surfactant solution (green curve) and the measured BHP (black curve) at the injector well for nine complete pilot SAG cycles. The injection rates during the pilot study were 520 and 470 rb/day for the surfactant solution and CO_2, respectively. The volumetric ratio of injected CO_2 relative to the total volume of CO_2 and surfactant injected was used to evaluate injected foam quality per cycle. The aim was to inject foam at 70% quality (0.70 gas fraction) per cycle, as determined in the laboratory studies. The foam qualities ranged from 61% to 71%, which was within the designed target.
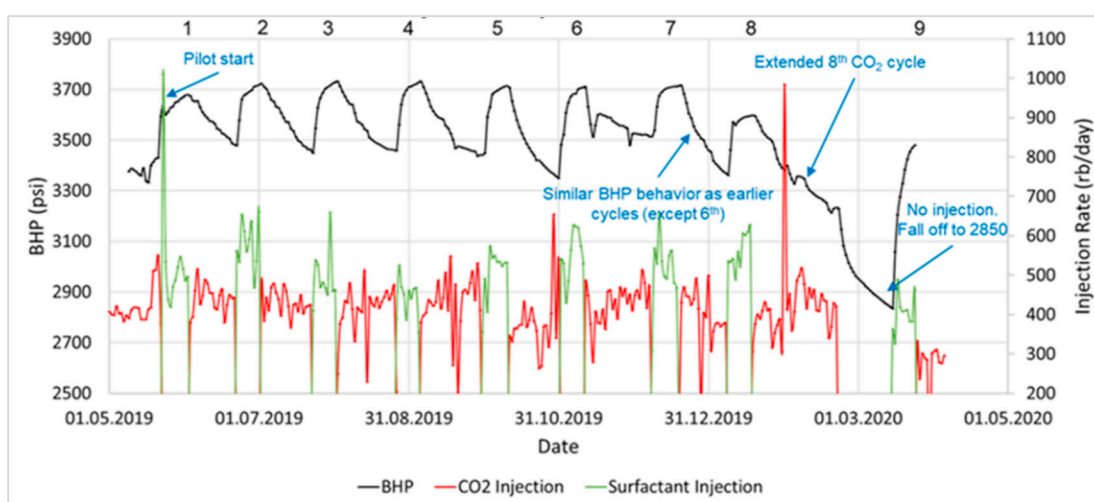

Figure 4. Plot showing the injection history along with measured bottom-hole pressures during the 9 SAG cycles.

8. Base Case Simulations

The simulated BHP was compared with actual surveys to evaluate foam generation and CO_2 mobility reduction. Figure 5 shows the surfactant-alternating gas (SAG) simulation

results, assuming the base case foam parameters (red curve). As can be seen in this plot, the simulated pressures were significantly higher than the measured BHP (black curve). In addition, the simulated pressures assuming a water-alternating gas (WAG) scenario are shown (blue curve), which were slightly lower but more consistent with the measured pressures, suggesting a weaker foam than that expected.
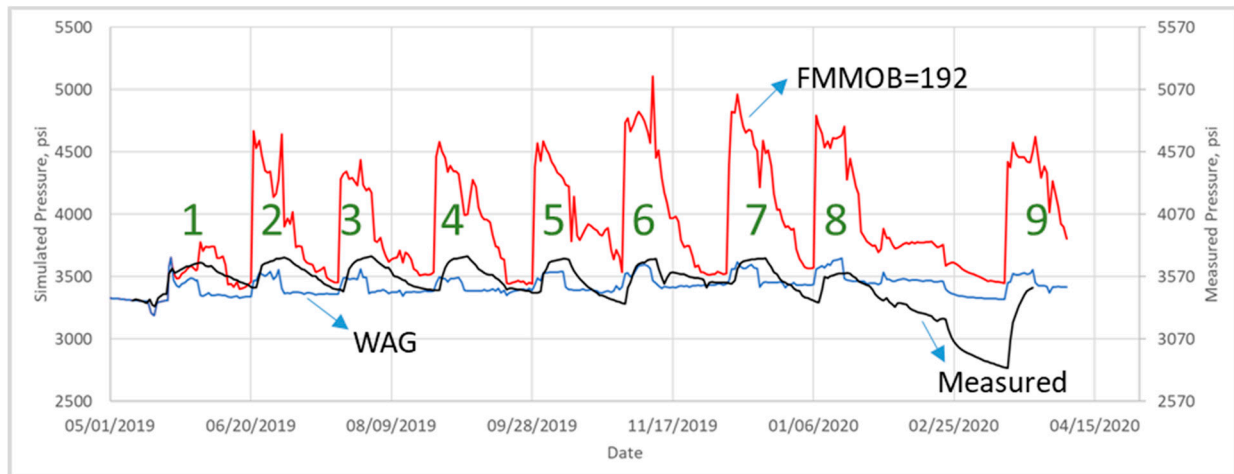

Figure 5. Simulated pressures using base case foam parameters.

The radial simulation model assumed a constant effect of nearby wells, and this may only be true for limited times. To check this assumption, the injection and production rates within the pilot pattern were also plotted. Figure 6 shows the total injection rates for the pilot pattern. As can be seen from this plot, the total CO_2 injection rate increased during Cycles 6 and 7 and decreased during Cycles 8 and 9. This is important since the radial well model only simulated the central injector and did not consider the effects of injection/production on the nearby wells. These non-steady conditions are addressed later in the transient analysis section.
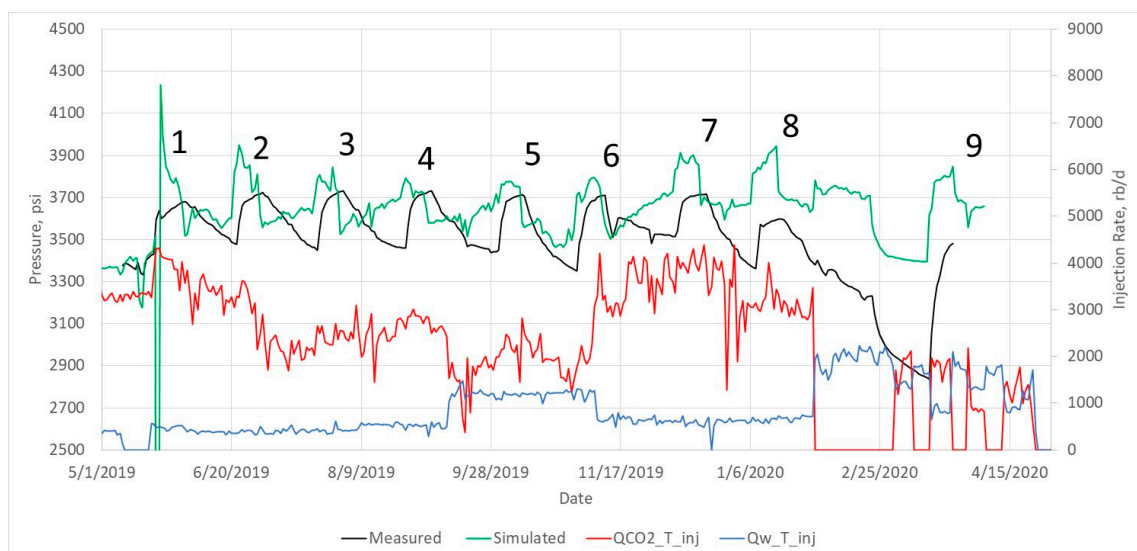

Figure 6. Total injection and BHP measured for the pilot study. The black curve shows the measured bottom-hole pressure data. The green curve shows simulated results from the base case model. Values for CO_2 and water injection rates (red and blue curves) are indicated on the secondary axis (rb/d).

9. Sensitivity Studies

Due to uncertainty in foam model parameters derived from laboratory data, sensitivity runs were set up to first test key foam model parameters. The following foam model parameters were adjusted for the sensitivity study:

- FMMOB: The reference mobility reduction factor;
- FMDRY: The limiting water saturation below which the foam is no longer effective;
- EPDRY: A weighting factor which controls the sharpness of the change in mobility;
- FOAMSO: The maximum oil saturation above which foam is no longer effective.

Table 4 shows the parameter ranges for the sensitivity study.

Table 4. Foam sensitivity parameters.

Simulation Run	FMMOB	FMDRY	EPDRY	FOAMFSO
Base Case	**192**	**0.4**	**84**	**0.28**
S1	92			
S2	19			
S3		0.45		
S4		0.35		
S5			42	
S6			168	
S7				0.18
S8				0.38

Figure 7 shows the sensitivity to foam strength parameters (FMMOB). As expected, the simulated pressures agreed better with the measured BHP, because the foam strength was controlled by the set FMMOB value. Sensitivity simulations for other foam parameters showed less of an impact; therefore, they are not shown here. These results clearly show that the foam was formed down-hole, and it was weaker than expected.
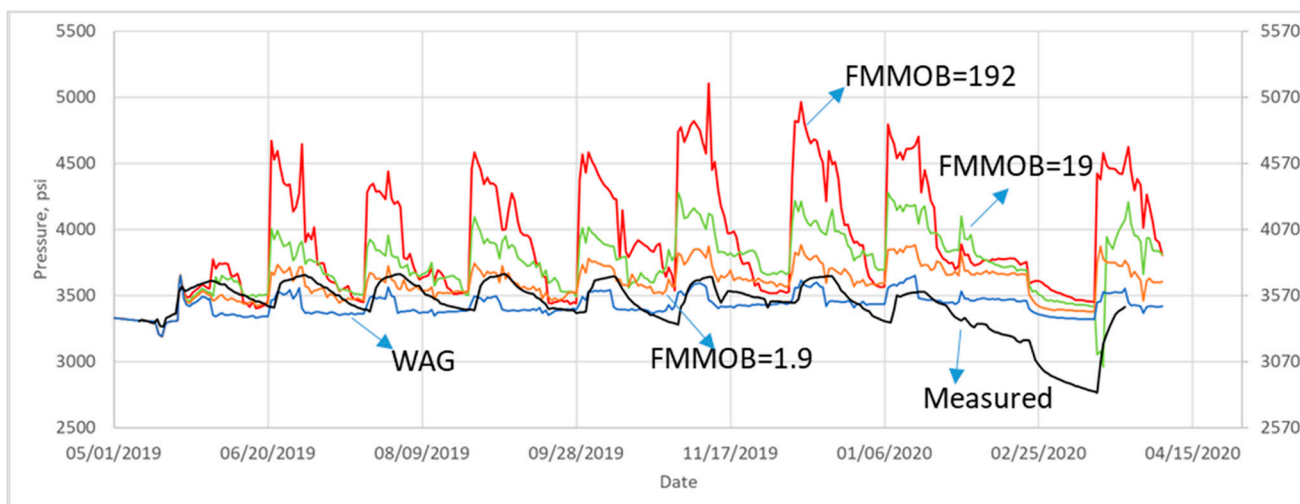

Figure 7. Simulated pressures using different foam strength parameters.

10. Transient Pressure Analysis

An alternative analysis was carried out using the pressure changes (instead of the absolute pressures) for each cycle. This analysis showed consistent results for both surfactant and CO_2 injection periods. Transient analysis represented a useful tool to analyze unsteady-state flow at the pilot injector. Figure 8 shows dP/dT over time for the first five SAG cycles. Delta pressure (dP) and delta temperature (dT) values were calculated by subtracting the absolute values from the last stabilized pressure and temperature before each injection cycle, a technique widely used in transient pressure analysis. Similarly, delta

t (dt) refers to the differential time from the start of a particular injection cycle. Differential pressure (dP) increased for each surfactant cycle, which may be related to a foam bank developing further into the reservoir. The dP values were in the order Cycle 1 < Cycle 2 < Cycle 3 < Cycle 4 < Cycle 5.
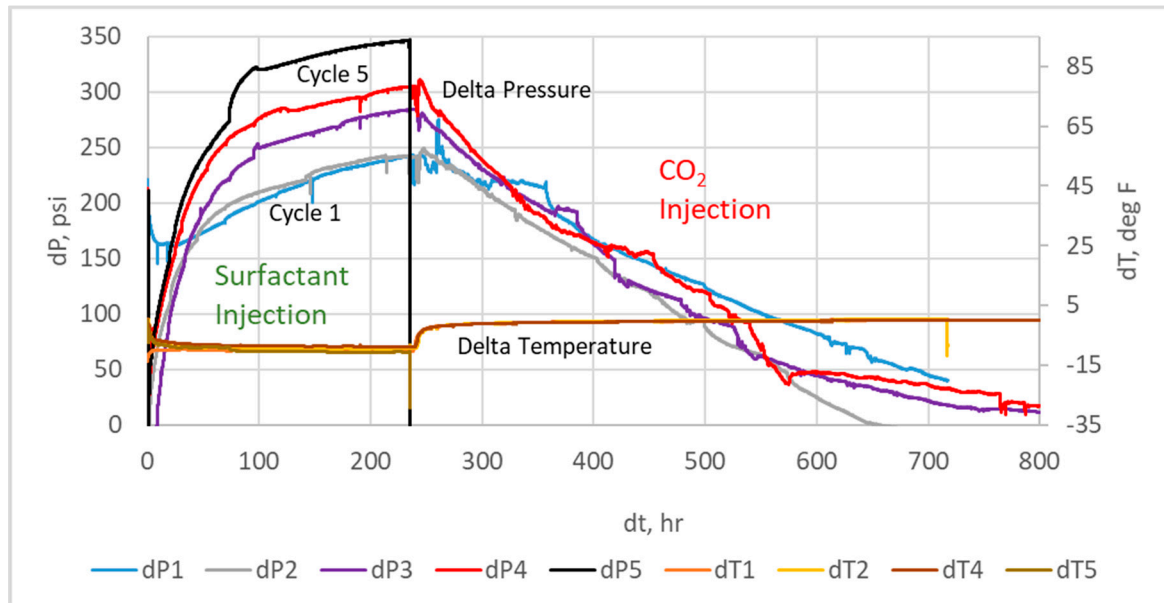

Figure 8. Transient pressures and temperatures for the first five SAG cycles. dP1 corresponds to slug 1, dP2 to slug 2, and so on.

The increased BHP during surfactant cycles could also be related to relative permeability and/or viscosity effects. A WAG was run at the end of the pilot to rule this out. As shown in Figure 9, the dP during the final SAG cycle (red curve) was higher than the dP observed during the final WAG (blue curve). The higher dP of the SAG cycles compared with the WAG indicated reduced the mobility during the SAG cycles and confirmed foam generation.
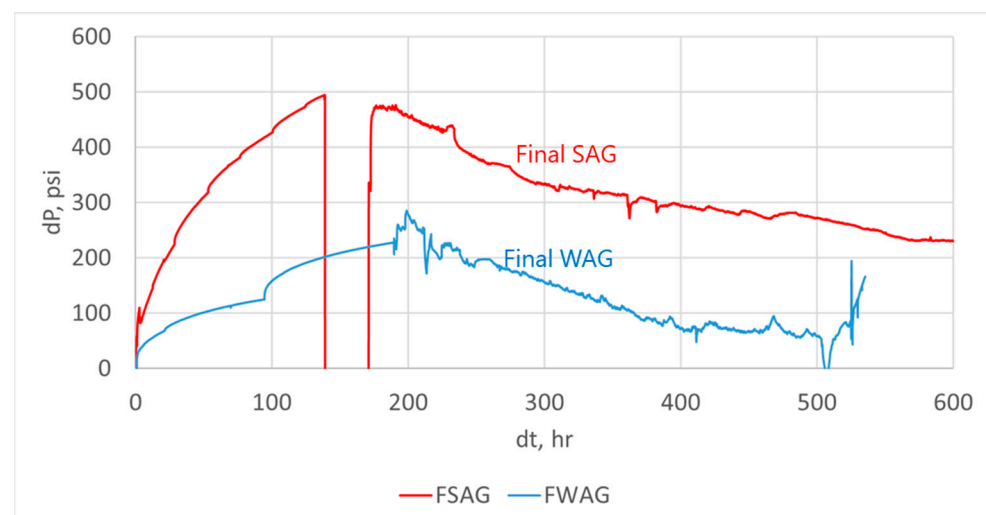

Figure 9. Transient bottom-hole pressure (dP) versus injection time (dt) for the final SAG cycle (red curve) and for the WAG cycle (blue curve).

The transient analysis was also applied to CO_2 injection periods independently. These results, along with the extended fall-off period, are shown in Figure 10.
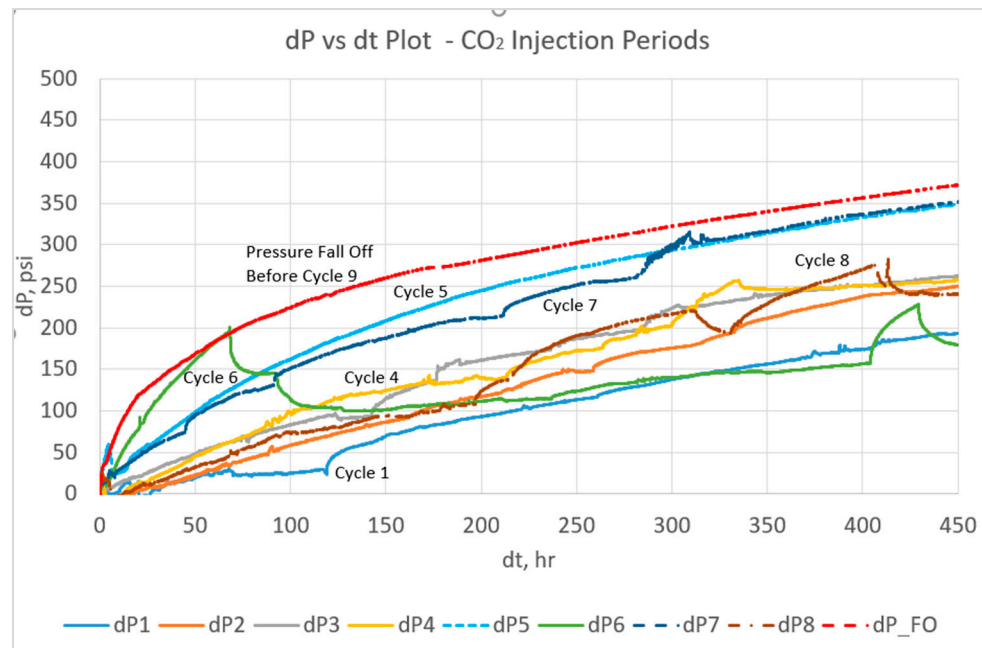
Figure 10. Transient analysis of CO_2 injection periods for the first 8 cycles. Additionally, the pressure fall-off results before Cycle 9 are shown.

11. Fall-Off Comparison

Due to operational reasons, the central injector was shut in for an extended period before Cycle 9. This created a fall-off test, which was also used to test different foam scenarios. Figure 11 shows the simulated results versus the measured dP/dT response during this fall-off period. As indicated, the simulated case with a lower FMMOB value (gray curve) followed the measured response more closely than the cases with higher mobility reduction (yellow and blue curves). In addition, the WAG case had a much lower pressure response, compared with the cases with foam and the observed data. This may indicate that a relatively weak foam was generated in the reservoir.
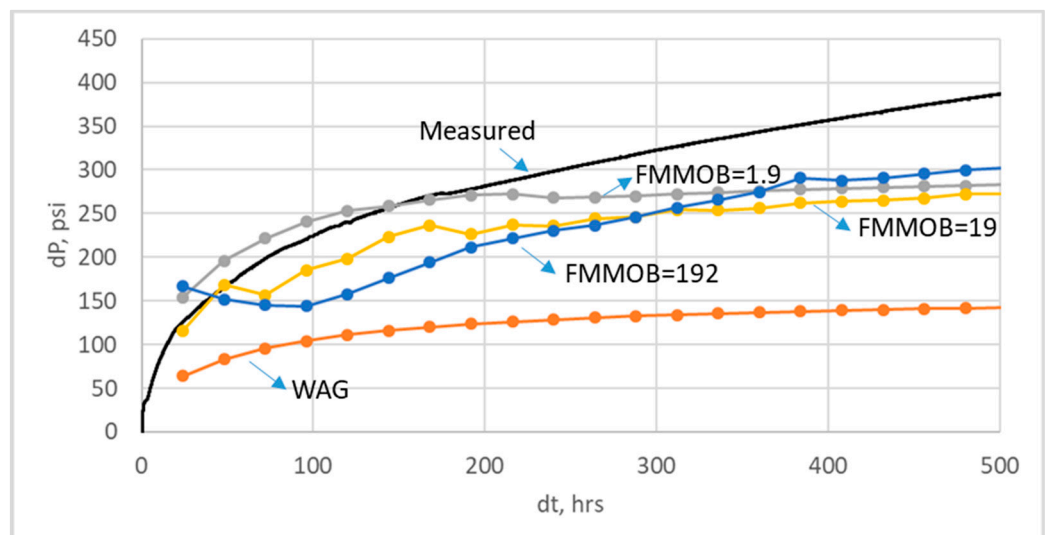

Figure 11. Simulated transient pressures during the fall-off period with different foam strength parameters.

12. Transient Surfactant and CO_2 Injection Comparisons

Transient data were also used to compare the model pressure response with the measured pressures during surfactant and CO_2 injection periods. These are shown in

Figures 12 and 13, respectively. These comparisons showed similar results to those observed during the fall-off period, suggesting weak foam strength.
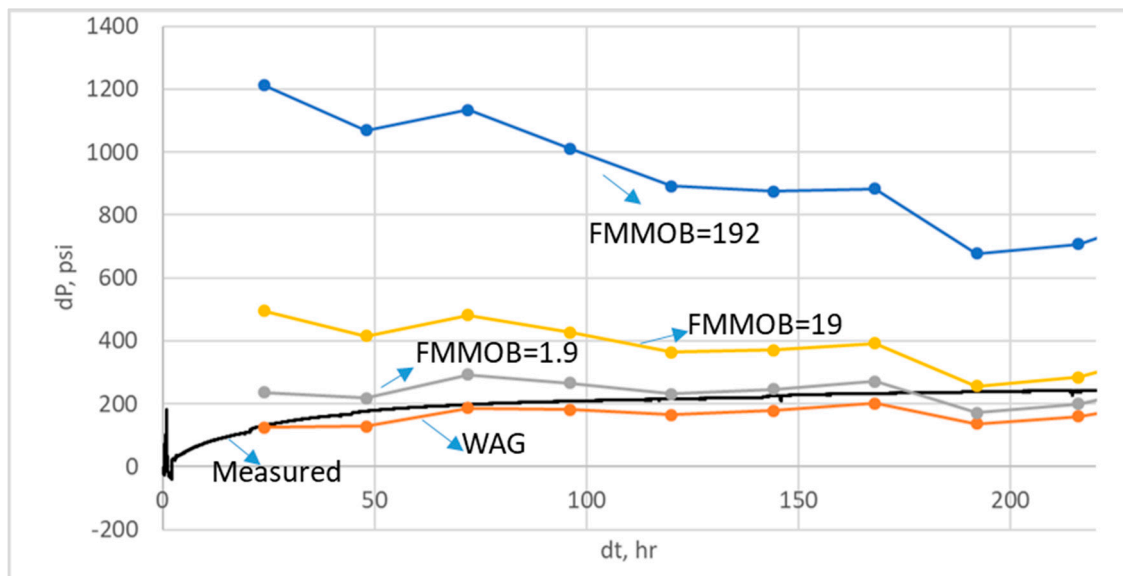

Figure 12. Simulated transient pressures of CO_2 injection during Cycle 2 with different foam strength parameters.
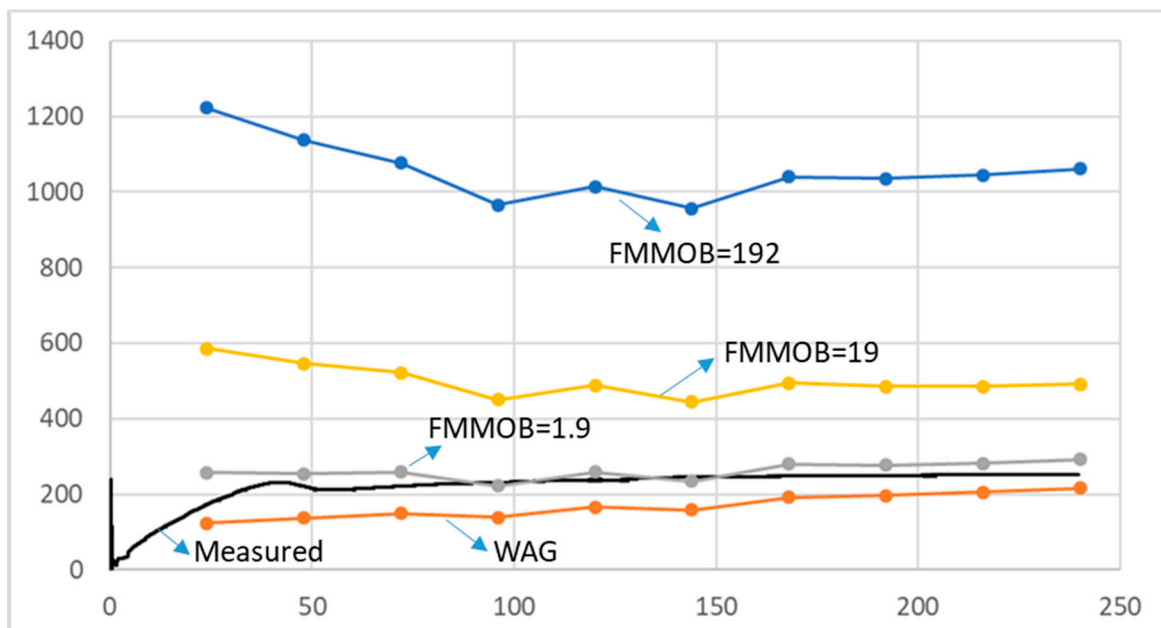

Figure 13. Simulated transient pressures of CO_2 injection during Cycle 8 with different foam strength parameters.

13. Foam Propagation

One of the important objectives of this study was to determine the foam propagation distance/rate if foam had formed. For this, a history-matched simulation model with tuned parameters was used. The simulator modeled foam as an effective concentration of surfactant transported in the gas (CO_2) phase. Figure 14 shows the simulated foam propagation for the weak foam case (FMMOB = 1.9) at the end of each surfactant/CO_2 cycle for Cycles 1, 5 and 8. These plots clearly indicate that foam had advanced deep in high-permeability layers during the pilot study.
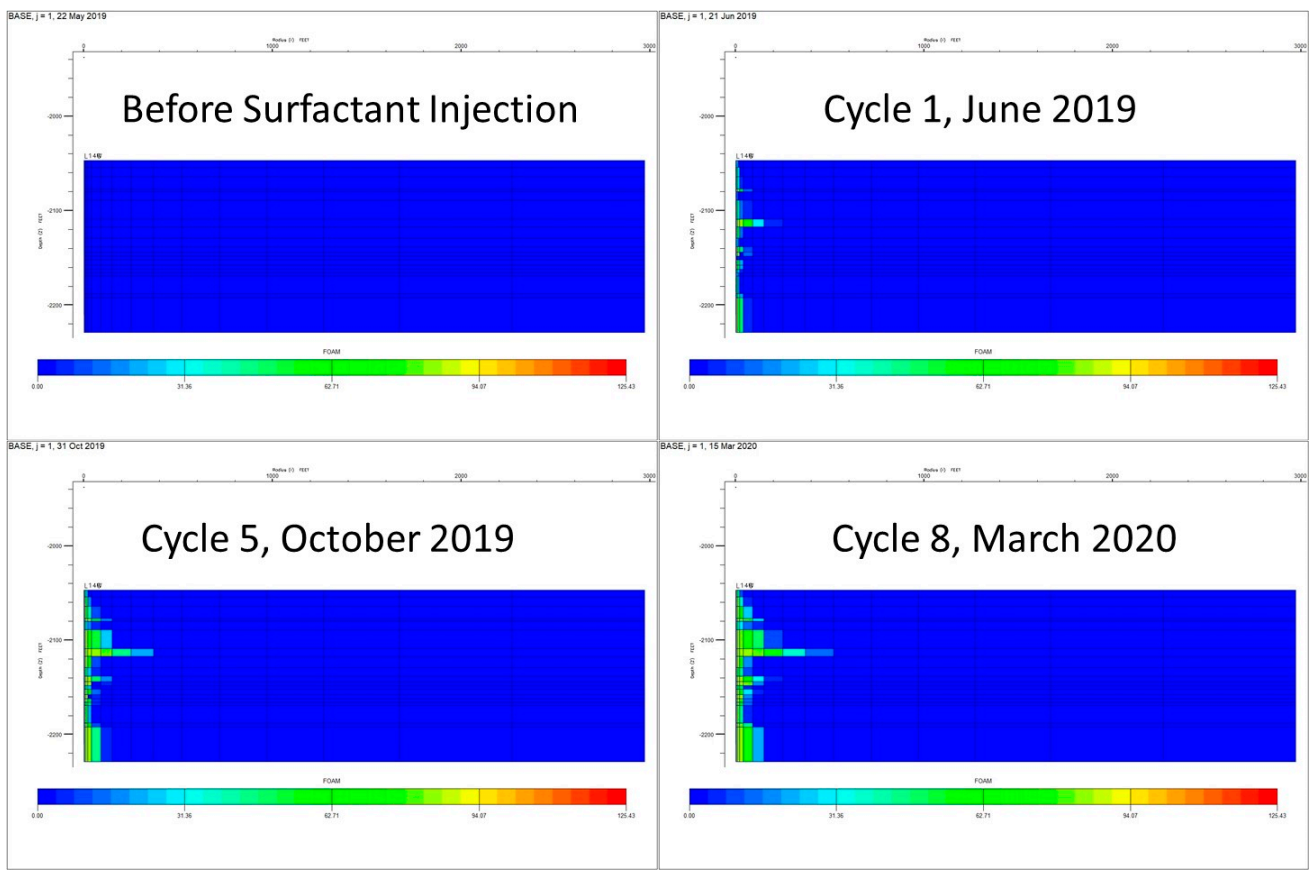
Figure 14. Cross-sectional (r-z) plot showing simulated foam concentrations for the weak foam case (FMMOB = 1.9) at the end of Cycles 1, 5 and 8.

14. Results and Discussion

The simulation model assuming the base case foam parameters for the SAG scenario gave significantly higher pressures than the measured pressures. This clearly shows that the simulated foam (or resistance) was stronger than that which occurred in reservoir conditions. The simulated WAG scenario (or no foam case) provided a lower bound for these pressures; therefore, based on the history-matched results, it could be concluded that the generated foam was weaker than expected.

Transient analysis showed that the temperature response was quite similar during all SAG cycles. On the other hand, differential pressures consistently increased during periods of surfactant injection and decreased during the subsequent CO_2 injection periods. The pressure increase (buildup) during surfactant injection clearly suggests the development of a mobility bank in the reservoir. Transient analysis also showed that the differential pressures during the SAG cycles were higher than the pressures observed during the WAG cycle. This revealed foam generation and reduced CO_2 mobility during this pilot development.

History matching using different foam parameters showed that a large reduction in the foam mobility reduction factor (FMMOB) was needed to match the measured bottom-hole pressure data. Other foam parameters were also selectively adjusted, and results showed they had less of an impact on the overall pressure match. However, considering the non-unique nature of parameter estimation [28], the effects of these foam parameters should be addressed by more direct indicators of foam saturation, such as resistivity measurements [16].

The effectiveness of the foam could also be independently determined by improvements in the overall oil recovery against the base water/gas injection within the pilot area. A production analysis conducted after the pilot indicated a significant increase in both cumulative oil and water production compared to the baseline period before the pilot.

However, a large increase in water production was also observed, which may be related to a fracturing campaign conducted on pilot wells at the onset of the pilot. Therefore, no definite conclusions were drawn from this pilot with regard to the effectiveness of the foam based on the oil production increase.

15. Conclusions

In this study, we presented a novel technique to study the development of foam in reservoir conditions. The method was used to assess the effectiveness of CO_2 foam in a pilot study conducted in the East Seminole Field, Permian Basin, West Texas. In the selected pilot area, foam was utilized to reduce CO_2 mobility to improve sweep efficiency, oil recovery, and CO_2 storage potential. Injection pressure and temperature data were used to evaluate the reservoir response during various surfactant, CO_2 and water injection periods. Transient analyses were conducted for all SAG cycles, as well as one WAG cycle. A high-resolution two-dimensional radial flow model was used to history-match the measured differential pressures.

The radial model proved to be useful for assessing the reservoir foam strength during this pilot study. Although the pressure data alone may not be sufficient to describe the complex physics of in situ foam generation, this study shows that it is a strong indicator of foam strength. In this pilot, it appears that the reservoir foam strength was weaker than expected based on laboratory measurements.

The proposed method of transient analysis has been found to be quite useful in assessing the development and progression of foam in the reservoir. This analysis showed a consistent increase during all SAG cycles. In addition, differential pressures during the SAG periods were higher than those observed during a comparable WAG cycle. This revealed foam generation and reduced CO_2 mobility during the pilot. Based on the detailed comparisons and the transient analysis of measured bottom-hole pressure data, it could be concluded that foam was generated down-hole. However, the history-matched foam model was weaker than that expected based on laboratory studies.

Sensitivity studies show that the foam mobility reduction factor (FMMOB) is the most dominant parameter. Based on the history-matched model simulations, it could be concluded that the foam significantly advanced in high-permeability layers during this pilot study.

Nomenclature

f_g	Gas fraction or foam quality
cP	Centipoise
K	Permeability
mD	Millidarcy
MPa	Megapascal
$Psig$	Pound per square inch, gauge
$Mscf$	Thousand standard cubic feet
^0API	American Petroleum Institute gravity
rb/day	Reservoir barrels per day
Mscf/day	Thousand standard cubic feet per day
S_{or}	Residual oil saturation, fraction of pore volume
$fmmob$	Foam model, maximum gas mobility reduction factor
$fmdry$	Foam model parameter in Fwater
$epdry$	Foam model parameter in Fwater
$fmsurf$	Foam model parameter in Fsurf
$epsurf$	Foam model parameter in Fsurf
FM	Foam model, mobility reduction factor
k_{rg}^{nf}	Gas relative permeability with no foam

Abbreviations

$CCUS$	Carbon capture, utilization, and storage
CCS	Carbon capture and storage
EOR	Enhanced oil recovery
SAG	Surfactant-alternating gas
WAG	Water-alternating gas
$DHPG$	Down-hole pressure gauge
BHP	Bottom-hole pressure
MPZ	Main producing zone
ROZ	Residual oil zone
BT	Breakthrough
$Wt\ \%$	Weight percentage
GOR	Gas/oil ratio
MRF	Mobility reduction factor
$IWTT$	Interwell CO_2 tracer test
PV	Pore volume

SI Metric Conversion Factors	
Acre $\times$ 4.046873	E + 03 = m^2
^{o}API 141.5/(131.5 + ^{o}API)	= g/cm^3
bbl $\times$ 1.589873	E − 01 = m^3
cp $\times$ 1.0	E − 03 = Pa·s
^{o}F (^{o}F − 32)/1.8	= °C
ft $\times$ 3.048	E − 01 = m
psi $\times$ 6.894757	E + 00 = kPa

References

1. Enick, R.M.; Olsen, D.K.; Ammer, J.R.; Schuller, W. Mobility and Conformance Control for CO2 EOR via Thickeners, Foams, and Gels—A Literature Review of 40 Years of Research and Pilot Tests; SPE-154122-MS. In Proceedings of the SPE Improved Oil Recovery Symposium, Tulsa, OK, USA, 14–18 April 2012. [CrossRef]
2. Heller, J.P. Onset of Instability Patterns between Miscible Fluids in Porous Media. *J. Appl. Phys.* **1966**, *37*, 1566–1579. [CrossRef]
3. Heller, J.P.; Boone, D.A.; Watts, R.J. Field Test of CO2-Foam Mobility Control at Rock Creek; SPE-14395. In Proceedings of the SPE 60th Annual Technical Conference and Exhibition, Las Vegas, NV, USA, 22–25 September 1985.
4. Chou, S.I.; Vasicek, S.L.; Pisio, D.L.; Jasek, D.E.; Goodgame, J.A. CO$_2$ Foam Field Trial at North Ward Estes. In Proceedings of the 67th SPE Annual Technical Conference and Exhibition, Washington, DC, USA, 4–7 October 1992.

5. Martin, F.D.; Heller, J.P.; Weiss, W.W.; Tsau, J.S. CO2-Foam Field Verification Pilot Test at EVGSAU Injection Project Phase 1: Project Planning and Initial Results; SPE/DOE-24176. In Proceedings of the SPE Improved Oil Recovery Conference, Tulsa, OK, USA, 22–24 April 1992.

6. Hoefner, M.L.; Evans, E.M. CO_2 Foam: Results from Four Developmental Field Trials. *SPE Reserv. Eng.* **1995**, *10*, 273–281. [CrossRef]

7. Martin, F.D.; Stevens, J.E.; Harpole, K.J. CO2-Foam Field Test at the East Vacuum Grayburg/San Andres Unit. *SPE Reserv. Eng.* **1995**, *10*, 266–272. [CrossRef]

8. Leeftink, T.N.; Latooij, C.A.; Rossen, W.R. Injectivity errors in simulation of foam EOR. *J. Pet. Sci. Eng.* **2015**, *126*, 26–34. [CrossRef]

9. Rossen, W.R. Foams in Enhanced Oil Recovery. In *Foams Theory, Measurements, and Applications*; Prud'homme, R.K., Khan, S.A., Eds.; Marcel Dekker, Inc.: New York, NY, USA, 1996; Volume 57, Chapter 11; pp. 414–464.

10. Falls, A.H.; Hirasaki, G.J.; Patzek, T.W.; Gauglitz, D.A.; Miller, D.D.; Ratulowski, T. Development of a Mechanistic Foam Simulator: The Population Balance and Generation by Snap-Off. *SPE Reserv. Eng.* **1988**, *3*, 884–892. [CrossRef]

11. Schramm, L.L. *Foams: Fundamentals and Applications in the Petroleum Industry*; American Chemical Society: Washington, DC, USA, 1994.

12. Jian, G.; Zhang, L.; Da, C.; Puerto, M.; Johnston, K.P.; Biswal, S.L.; Hirasaki, G.J. Evaluating the Transport Behavior of CO_2 Foam in the Presence of Crude Oil under High-Temperature and High-Salinity Conditions for Carbonate Reservoirs. *Energy Fuels* **2019**, *33*, 6038–6047. [CrossRef]

13. Rognmo, A.; Heldal, S.; Fernø, M. Silica nanoparticles to stabilize CO2-foam for improved CO_2 utilization: Enhanced CO2 storage and oil recovery from mature oil reservoirs. *Fuel* **2018**, *216*, 621–626. [CrossRef]

14. Haroun, M.; Mohammed, A.M.; Somra, B.; Punjabi, S.; Temitope, A.; Yim, Y.; Anastasiou, S.; Abu Baker, J.; Haoge, L.; Al Kobaisi, M.; et al. Real-Time Resistivity Monitoring Tool for In-Situ Foam Front Tracking. In Proceedings of the Abu Dhabi International Petroleum Exhibition & Conference, Abu Dhabi, United Arab Emirates, 13 November 2017. [CrossRef]

15. Gargar, N.K.; Mahani, H.; Rehling, J.G.; Vincent-Bonnieu, S.; Kechut, N.I.; Farajzadeh, R. Fall-Off Test Analysis and Transient Pressure Behavior in Foam Flooding. In Proceedings of the IOR 2015-18th European Symposium on Improved Oil Recovery. European Association of Geoscientists & Engineers, Dresden, Germany, 16 April 2015.

16. Karakas, M.; Aminzadeh, F. Optimization of CO2-Foam Injection through Resistivity and Pressure Measurements. In Proceedings of the SPE Western Regional Meeting, Garden Grove, CA, USA, 22 April 2018. [CrossRef]

17. Alcorn, Z.P.; Fredriksen, S.B.; Sharma, M.; Rognmo, A.U.; Føyen, T.L.; Fernø, M.; Graue, A. An Integrated Carbon-Dioxide-Foam Enhanced-Oil-Recovery Pilot Program with Combined Carbon Capture, Utilization, and Storage in an Onshore Texas Heterogeneous Carbonate Field. *SPE Reserv. Eval. Eng.* **2019**, *22*, 1449–1466. [CrossRef]

18. Alcorn, Z.P.; Føyen, T.; Zhang, L.; Karakas, M.; Biswal, S.L.; Hirasaki, G.; Graue, A. CO_2 Foam Field Pilot Design and Initial Results; SPE-200450-MS. In Proceedings of the SPE Improved Oil Recovery Conference 2020, Virtual, 30 August 2020.

19. Rognmo, A.U.; Fredriksen, S.B.; Alcorn, Z.P.; Sharma, M.; Føyen, T.; Eide, G.A.; Fernø, M. Pore-to-Core EOR Upscaling for CO_2 Foam for CCUS. *SPE J.* **2019**, *24*, 2793–2803. [CrossRef]

20. Ma, K.; Lopez-Salinas, J.L.; Puerto, M.C.; Miller, C.A.; Biswal, S.L.; Hirasaki, G.J. Estimation of Parameters for the Simulation of Foam Flow through Porous Media. Part 1: The Dry-Out Effect. *Energy Fuels* **2013**, *27*, 2363–2375. [CrossRef]

21. Sharma, M.; Alcorn, Z.; Fredriksen, S.; Fernø, M.; Graue, A. Numerical Modeling Study for Designing CO2-foam Field Pilot. In Proceedings of the IOR 2017—19th European Symposium on Improved Oil Recovery, Stavanger, Norway, 24 April 2017. [CrossRef]

22. Sharma, M.; Alcorn, Z.P.; Fredriksen, S.B.; Rognmo, A.U.; Ferno, M.A.; Skjaeveland, S.M.; Graue, A. Model calibration for forecasting CO2-foam EOR field pilot performance in a carbonate reservoir. *Pet. Geosci.* **2019**, *26*, 141–149. [CrossRef]

23. Zeng, Y.; Muthuswamy, A.; Ma, K.; Wang, L.; Farajzadeh, R.; Puerto, M.; Vincent-Bonnieu, S.; Eftekhari, A.A.; Wang, Y.; Da, C.; et al. Insights on Foam Transport from a Texture-Implicit Local-Equilibrium Model with an Improved Parameter Estimation Algorithm. *Ind. Eng. Chem. Res.* **2016**, *55*, 7819–7829. [CrossRef]

24. Rossen, W.R.; Zeilinger, S.C.; Shi, J.-X.; Lim, M.T. Simplified Mechanistic Simulation of Foam Processes in Porous Media. *SPE J.* **1999**, *4*, 279–287. [CrossRef]

25. Cheng, L.; Reme, A.; Shan, D.; Coombe, D.; Rossen, W. Simulating Foam Processes at High and Low Foam Qualities; SPE-59287-MS. In Proceedings of the SPE/DOE Improved Oil Recovery Symposium, Tulsa, OK, USA, 3 April 2000. [CrossRef]

26. Farajzadeh, R.; Andrianov, A.; Krastev, R.; Hirasaki, G.; Rossen, W. Foam–oil interaction in porous media: Implications for foam assisted enhanced oil recovery. *Adv. Colloid Interface Sci.* **2012**, *183–184*, 1–13. [CrossRef] [PubMed]

27. Law, D.H.S.; Yang, Z.M.; Stone, T.W. Effect of the Presence of Oil on Foam Performance: A Field Simulation Study; SPE-18421-PA. *SPE Reserv. Eng.* **1992**, *7*, 228–236. [CrossRef]

28. Ma, K.; Farajzadeh, R.; Lopez-Salinas, J.L.; Miller, C.A.; Biswal, S.L.; Hirasaki, G.J. Non-uniqueness, Numerical Artifacts, and Parameter Sensitivity in Simulating Steady-State and Transient Foam Flow through Porous Media. *Transp. Porous Media* **2014**, *102*, 325–348. [CrossRef]